Compensation temperatures and exchange bias in La$_{1.5}$Ca$_{0.5}$CoIrO$_6$

L. T. Coutrim,[1] E. M. Bittar,[2] F. Stavale,[2] F. Garcia,[2] E. Baggio-Saitovitch,[2] M. Abbate,[3] R. J. O. Mossanek,[3] H. P. Martins,[3]
D. Tobia,[4] P. G. Pagliuso,[4] and L. Bufaiçal[1,*]

[1]*Instituto de Física, Universidade Federal de Goiás, 74001-970, Goiânia, GO, Brazil*
[2]*Centro Brasileiro de Pesquisas Físicas, 22290-180, Rio de Janeiro, RJ, Brazil*
[3]*Universidade Federal do Paraná, 19044, 81531-990 Curitiba, PR, Brazil*
[4]*Instituto de Física "Gleb Wataghin", UNICAMP, 13083-859, Campinas, SP, Brazil*

We report on the study of magnetic properties of the La$_{1.5}$Ca$_{0.5}$CoIrO$_6$ double perovskite. Via ac magnetic susceptibility we have observed evidence of weak ferromagnetism and reentrant spin glass behavior on an antiferromagnetic matrix. Regarding the magnetic behavior as a function of temperature, we have found that the material displays up to three inversions of its magnetization, depending on the appropriate choice of the applied magnetic field. At low temperature, the material exhibits exchange bias effect when it is cooled in the presence of a magnetic field. Also, our results indicate that this effect may be observed even when the system is cooled at zero field. Supported by other measurements and also by electronic structure calculations, we discuss the magnetic reversals and spontaneous exchange bias effect in terms of magnetic phase separation and magnetic frustration of Ir^{4+} ions located between the antiferromagnetically coupled Co ions.

I. INTRODUCTION

Magnetic frustration emerges from competing magnetic interactions and degenerate multivalley ground states [1]. An example of such systems are the spin glasses (SG), in which the interactions between magnetic moments are in conflict with each other due to the presence of frozen-in structural disorder. The intriguing physical phenomena underlying the SG behavior have led to great interest in these materials since the 1970's. The development of theories to model the SG found its applicability in a wide variety of research fields, from real glasses to neural networks and protein folding [2,3]. Despite the great scientific interest and intense research over the last decades, the underlying physics that governs the SG phenomena is far from being well understood.

The canonical example of an SG type material is an intermetallic alloy in which a few percent of magnetic ions are dispersed arbitrarily in a nonmagnetic matrix. These magnetic atoms are therefore separated by incidental distances, and thus the RKKY (Ruderman-Kittel-Kasuya-Yosida) interaction allows the coupling energy to have random sign. This class of systems corresponds to the historical discovery of SG, which traces back to the studies of strongly diluted magnetic alloys and the Kondo effect [3].

Later on, SG have been identified within other systems, such as insulating intermetallics, layered thin films and magnetic oxides. For the later class of materials, is important to mention the geometric frustrated pyrochlores [4,5] and the extensively studied Co/Mn-based perovskites [6–8]. For these A(Co,Mn)O$_3$ materials, the SG-like behavior is usually ascribed to the phase segregation and inhomogeneity of the compounds, and the dynamical process of magnetic relaxation being related to the growth and interactions of magnetic clusters [2,9]. Many of these cobaltites and manganites exhibit the interesting exchange-bias (EB) effect, for which there is a

shift of the magnetization as a function of the applied magnetic field [$M(H)$] curve in respect to its center. This phenomena is usually attributed to the induced exchange anisotropy at the interface between antiferromagnetic (AFM) and ferromagnetic (FM)/ferrimagnetic (FIM) phases in heterogeneous systems [10], and it has also been observed at FM/FIM/AFM-SG interfaces [11,12]. It is commonly observed in multilayered systems, although also found in bulk materials with competing magnetic interactions with undefined magnetic interfaces between regions with AFM or FIM interactions [10].

We recently reported the structural and magnetic characterization of the La$_{2-x}$Ca$_x$CoIrO$_6$ double perovskite series [13]. For La$_2$CoIrO$_6$, the transition-metal ions valences are reported to be Co^{2+} and Ir^{4+} [14]. Our results show that La^{3+} to Ca^{2+} substitution leads to Co valence changes, and La$_{1.5}$Ca$_{0.5}$CoIrO$_6$ presents both Co^{2+} and Co^{3+} in high-spin configuration. Moreover, it presents the two key ingredients to achieve a SG state, which are different competing magnetic interactions and disorder [2,3,13].

In the course of studying the magnetic properties of La$_{1.5}$Ca$_{0.5}$CoIrO$_6$, we have observed a reentrant spin glass (RSG)-like state, i.e., there is a conventional magnetic ordering and, at lower temperature (T), the system achieves the SG state concomitantly to other magnetic phases. This behavior is ascribed to the Ir magnetic frustration due to Co AFM coupling and to the magnetic phase separation induced by the antisite disorder (ASD) at the transition-metal sites.

This RSG state is intrinsically related to the EB effect observed for La$_{1.5}$Ca$_{0.5}$CoIrO$_6$. Another important feature observed is that, for an appropriate choice of the applied dc magnetic field (H_{dc}), the compound can reverse its magnetization up to three times in the T-dependent magnetization measurements.

In this work we report the investigation of the magnetic behavior of La$_{1.5}$Ca$_{0.5}$CoIrO$_6$. Using ac magnetic susceptibility measurements we have observed that the system exhibit conventional magnetic orderings at $T \sim 90$ K and a spin glass transition at $T \simeq 27$ K, confirming its RSG state at

*lbufaical@ufg.br

low T. The dc magnetization measurements revealed that the high-T anomaly is in fact associated with two conventional magnetic transitions, the AFM and FM phases of Co ions. The compensation temperatures in the T-dependent magnetization measurements and the spontaneous EB effect in the isothermal magnetization measurements were investigated in detail. Studies of x-ray absorption near-edge structure (XANES), x-ray magnetic circular dichroism (XMCD), x-ray photoelectron spectroscopy (XPS) and band-structure calculations were also carried out. These data corroborate our argument that the magnetization reversals and zero-field cooled (ZFC) exchange bias effect observed for $La_{1.5}Ca_{0.5}CoIrO_6$ can be both understood in terms of the same underlying mechanism, i.e., are due to the competing interactions of Co ions that leads to magnetic phase segregation and frustration of the Ir magnetic moments.

II. EXPERIMENTAL DETAILS

Polycrystalline samples of $La_{1.5}Ca_{0.5}CoIrO_6$ were prepared by the solid state reaction in a conventional tubular furnace and air atmosphere. Stoichiometric amounts of La_2O_3, CaO, Co_3O_4, and metallic Ir were mixed and heated at $650\,°C$ for 24 hours. Later, the samples were regrinded before a second step of 48 hours at $800\,°C$. Finally, the materials were grinded, pressed into pellets and heated at $975\,°C$ for two weeks. X-ray powder diffraction pattern revealed a single phase double perovskite structure with monoclinic $P2_1/n$ symmetry, with 9% of ASD at Co/Ir sites [13]. Magnetic data were collected on a commercial Physical Property Measurement System. AC magnetic susceptibility was measured with driving field $H_{ac} = 10$ Oe, at the frequency range of 10–10 000 Hz. Direct-current magnetization was measured at ZFC and field cooled (FC) modes. XPS experiments were performed using an ultra-high vacuum (UHV) chamber equipped with a SPECS analyzer PHOIBOS 150. XMCD and XANES measurements were performed in the dispersive x-ray absorption (DXAS) beam line at the Brazilian Synchrotron Light Laboratory (LNLS) [15]. The edge step normalization of the data was performed after a linear pre-edge subtraction and the regression of a quadratic polynomial beyond the edge, using the software ATHENA [16]. The band-structure calculations were performed using the WIEN2K software package [17].

III. RESULTS AND DISCUSSION

A. X-ray photoelectron spectroscopy (XPS)

Figure 1 shows the XPS spectra for $La_{1.5}Ca_{0.5}CoIrO_6$. All the results presented correspond to the use of monochromatic Al K_α x-ray radiation ($h\nu = 1486.6$ eV) using spectrometer pass energy (E_{pass}) of 15 eV. The spectrometer was previously calibrated using the Au $4f_{7/2}$ (84.0 eV), which results on a full-width-half-maximum of 0.7 eV, for a sputtered metallic gold foil. The samples were referenced by setting the adventitious carbon C 1s peak to 284.6 eV. Prior to mounting in UHV, samples were slightly polished and ultra-sonicated sequentially in isopropyl alcohol and water. The photoemission spectra were sequentially acquired after successive cycles of gentle Ar^+ sputtering (5×10^{-7} mbar Ar, 1 kV, 1 $\mu A/cm^2$, 10–15 seconds intervals) for hydrocarbons removal. All spectra
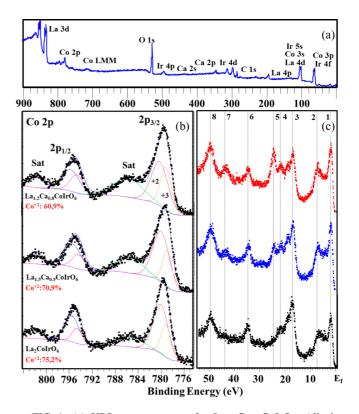

FIG. 1. (a) XPS survey spectra for $La_{1.5}Ca_{0.5}CoIrO_6$. All elements observed in the sample are indicated. (b) High-resolution Co $2p$ region for several Ca doping levels and the corresponding peak components fitting using the Shirley background and two Lorentzian-Gaussian peaks for Co^{2+} and Co^{3+} cations component. (c) The corresponding valence-band photoemission features and the main peaks indicated by line 1 and line 2, related to the high-spin state of the Co^{3+} cations.

shown correspond to 45-s Ar^+ sputtering at the ideally found conditions to avoid surface species reduction.

In Fig. 1(a), all elements found are indicated. We observe that residual carbon persist on the samples surface since the *in situ* sputtering has been employed at the optimal conditions to avoid chemical reduction. Particularly important is the careful analysis of the cobalt $2p$ region, which serves as a tool to assign Co cations sites and electronic configuration in several compounds [18–20]. Noteworthy, although XPS is most related to the surface chemical composition based on the limited photoelectrons inelastic mean free path in solids, because of the large mean free path of the cobalt photoelectrons (for $E_{Kin} \sim 700$ eV, about 1.5 nm) the spectra presented can certainly reveal additional information from buried layers. As reported extensively in the literature, the expected binding energies for Co^{3+} and Co^{2+} are 779.5 and 780.5 eV, respectively [21]. Importantly, depending on the cation symmetry one may observe satellite features related to charge-transfer mechanisms which appear significantly stronger for Co^{2+} in octahedral sites, in contrast to Co^{3+} in octahedral or Co^{2+} in tetrahedral sites. The differences has been discussed in the literature and arises from an enhanced screening of Co^{3+} due to a larger Co $3d$-O $2p$ hopping strength and a smaller charge-transfer energy compared to those in the Co^{2+} charge state [22]. In Fig. 1, the Co $2p$ XPS

spectra show prominent peaks at 779.6 and 795.3 eV related to the Co $2p_{3/2}$ and $2p_{1/2}$, respectively, in addition to the satellite feature located at 785.3 eV. The intense satellite is a clear signature of Co^{2+} in octahedral sites, most probably at a high-spin Co^{2+} configuration as observed for the cobalt monoxide [23].

The detailed analysis of the Co $2p$ region is however far from trivial, and the main peaks are known to be composed by multiplet splitting as described by Gupta and Sen [24], and extensively discussed in several recently studies [25,26]. Nevertheless, we have considered that the intensity of each spin-orbit component can be fitted using two curves related to the different Co cations and respective satellites since Co^{2+} and Co^{3+} are known to display well distinguish binding energies at about 780.1 and 779.6 eV [26]. The spectral analysis for $La_{1.5}Ca_{0.5}CoIrO_6$ compound employing two fitting components results on the assignment of Co^{2+} and Co^{3+} species located at binding energies and full-width-half-maximum of 780.1 (3.03) and 779.3 (1.89) eV, respectively. In order to compare the results obtained, the same procedure has been employed for La_2CoIrO_6 and $La_{1.2}Ca_{0.8}CoIrO_6$, as depicted in Fig. 1(b). The results indicate a Co^{2+}/Co^{3+} ratio of 2.33 for La_2CoIrO_6, 2.44 for $La_{1.5}Ca_{0.5}CoIrO_6$ and 3.03 for $La_{1.2}Ca_{0.8}CoIrO_6$. The increase of Co^{2+}/Co^{3+} ratio as a function of the Ca incorporation is expected and has served to test our fitting procedure. Certainly, the absolute amount can be hardly determined. However, the trend observed can fairly indicate the relative amount of Co^{3+} species in the compounds.

Furthermore, the photoemission spectra close to the valence band [Fig. 1(c)] is particularly helpful to distinguish the spin state of the Co cations since it display noticeable multiplet structure. The spectral features observed have been discussed by several authors in great detail for CoO, Co_3O_4, and more recently for $LaCoO_3$ [23,27,28]. The most important structure are those close to 1–8-eV range, indicated by line 1, which is expected for Co^{3+} in octahedral sites, and the one indicated by line 2, related to strong multiplet effects in the final state of Co^{3+} cations. Previous calculations and photoemission studies have shown that Co^{3+} in a purely, low-spin state is characterized by an intense peak close to 1 eV but broad features at energies ranging up to 8 eV [27]. In contrast, the $La_{1.5}Ca_{0.5}CoIrO_6$ compound displays two features peaking at lines 1 and 2, which suggest a Co^{3+} high-spin state.

The approximate 70%/30% proportion of Co^{2+}/Co^{3+} estimated from the XPS spectra is consistent to the effective magnetic moment, $\mu_{eff} = 5.8$ μ_B/f.u., obtained from the $H_{dc} = 500$ Oe $M(T)$ curve at the paramagnetic state (see below). Applying the usual equation for systems with two or more different magnetic ions [29]

$$\mu = \sqrt{\mu_1{}^2 + \mu_2{}^2 + \mu_3{}^2 + \dots} \qquad (1)$$

and using the standard magnetic moments of Ir^{4+} (1.73 μ_B), HS Co^{2+} (5.2 μ_B) and HS Co^{3+} (5.48 μ_B), yields

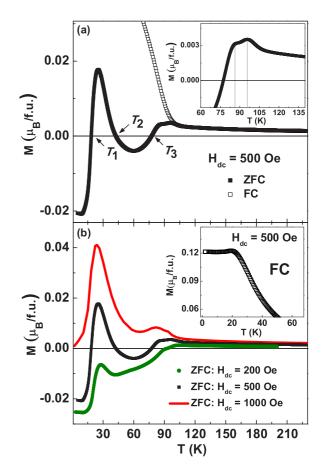$$\mu = \sqrt{0.7(5.2)^2 + 0.3(5.48)^2 + (1.73)^2} = 5.6\mu_B/f.u.. \quad (2)$$

FIG. 2. (a) ZFC and FC magnetization as a function of T for $La_{1.5}Ca_{0.5}CoIrO_6$ at $H_{dc} = 500$ Oe. The inset shows the magnified view of the AFM and FM transitions of Co ion. (b) ZFC magnetization as a function of T at $H_{dc} = 200$ Oe (solid circle), $H_{dc} = 500$ Oe (solid square), and $H_{dc} = 1000$ Oe (solid line). The inset shows the $H_{dc} = 500$ Oe FC curve at low-T.

The difference to the experimental value may be related to spin-orbit coupling (SOC) on Co ions, as already reported for similar compounds [14,27].

B. ac and dc magnetization versus T

Figure 2(a) presents the ZFC-FC magnetization curves for $H_{dc} = 500$ Oe, were two peaks can be clearly observed. The inset shows a magnified view of a stretch of the curve, where are evidenced two anomalies at $T \simeq 97$ and $\simeq 86$ K, associated to the magnetic ordering of the AFM and FM phases of Co ions, respectively, as it will be addressed later. The lower-T cusp at $\simeq 27$ K is due to a SG-like behavior, indicating a RSG phenomena. Since each peak is associated to a distinct mechanism, if an appropriate H_{dc} is applied in the opposite direction of the material's spontaneous magnetization (M_{sp}), the curve can be shifted down and display up to three reversals of its magnetic moment.

This scenario can be understood in terms of the AFM coupling of the Co ions that are located at their predicted site, resulting in the frustration of Ir^{4+} magnetic moment, and the development of a FM component caused by the ASD. Studies of XANES on Co K and Ir L_2, L_3 edges indicate

a Co mixed valence on $La_{1.5}Ca_{0.5}CoIrO_6$ (see Ref. [30]). Also, the XPS measurement discussed above suggests a proportion $\sim 70\%/30\%$ of high spin Co^{2+}/Co^{3+}. Ir maintains 4+ valence by La^{3+} to Ca^{2+} substitution. Reports of neutron powder diffraction studies on $La_{2-x}Sr_xCoIrO_6$ [14] and several closely related compounds (e.g., $La_{2-x}Sr_xCoRuO_6$ [38] and $LaBaCoIrO_6$ [39]) revealed AFM coupling of Co ions on these double perovskites, as predicted by the Goodenough-Kanamori-Anderson (GKA) rules [40]. Moreover, our electronic structure calculation results (see Ref. [30]) indicate the AFM ordering as the most stable structure for $La_{1.5}Ca_{0.5}CoIrO_6$. Therefore this spin orientation can be assumed for the majority of Co ions. Consequently, the Ir^{4+} located in between the AFM coupled Co^{2+} ions might be frustrated. However, the system exhibits 9% of ASD, which together with the 30% of Co^{3+} leads to other nearest neighbor interactions such as $Co^{2+}-O-Co^{3+}$, $Co^{3+}-O-Co^{3+}$, and $Ir^{4+}-O-Ir^{4+}$. The latter two couplings are AFM, as predicted by the GKA rules [40–42], but $Co^{2+}-O-Co^{3+}$ coupling is expected to be a short range FM interaction via double-exchange mechanism [27,43,44].

The resulting magnetic moment of $La_{1.5}Ca_{0.5}CoIrO_6$ can be estimated by the following argument. The main phase consists of AFM coupled Co^{2+} and frustrated Ir ions. Hence there is no contribution from the main phase to the resulting magnetization, as well as the AFM $Co^{3+}-O-Co^{3+}$ and $Ir^{4+}-O-Ir^{4+}$ couplings. To calculate the magnetization per formula unit, it must be taken into account that from the 30% of the Co^{3+} present in the system, in 9% it will permute to Ir site, giving rise to the FM $Co^{2+}-O-Co^{3+}$ interaction, which is the only from the interactions discussed above that is expected to contribute to the net magnetization. Using the standard magnetic moments of HS Co^{2+} and Co^{3+}, the FM contribution to the resulting magnetization can be estimated to be

$$M = 0.3 \times 0.09(0.5M_{Co^{3+}} + 0.5M_{Co^{2+}})$$
$$= 0.027(0.5 \times 5.48 + 0.5 \times 5.2) \quad (3)$$
$$= 0.14 \mu_B/f.u..$$

This result is very close to the low-T value of the FC magnetization observed on inset of Fig. 2(b), 0.12 μ_B/f.u., and to the remanent magnetization of $M(H)$ curve at 2 K ($M_R = 0.13 \mu_B$/f.u., see Fig. 6). It is also close to the total magnetic moment obtained from band structure calculation, $M = 0.15 \mu_B$/f.u. (see Ref. [30]). Surely, the above calculation is only an estimate, since it is not possible to establish the exact individual contribution of Co^{2+} and Co^{3+} magnetic moments. Also, the Co^{2+}/Co^{3+} proportion may vary a bit from that obtained from XPS, leading to the discrepancy between the observed and calculated values. The slightly larger experimental values may be also related to the contribution of the frozen SG ions, which were not taken into account in the calculation. The above approximation only takes into account the linear exchange of Ising moments. In a 3D system, other exchange pathways may play a role, resulting in a more complex picture, but also with competing FM and AFM interactions and perhaps even canted spins [5,40]. Hence, also for a 3D magnetic model, one would expect Ir^{4+} frustration. Frustration, along with the magnetic segregation due to ASD, fit very well the material's magnetic behavior.

The magnetic interactions discussed above can explain the curve of Fig. 2(a) as the following. After ZFC, at low T, there is only the M_{sp} related to the Co interactions, since the Ir moments are frustrated. The system's M_{sp} is here always chosen as opposite (negative) to H_{dc} direction (positive). Thus, applying H_{dc} in the opposite direction of M_{sp}, and ascending to higher-T there is the first compensation temperature at $T_1 \simeq 18$ K, due to the SG-spins alignment to H_{dc} direction. By increasing T there is the decrease of the SG correlation length, resulting in the second magnetization reversal at $T_2 \simeq 42$ K. With the further enhancement of the thermal energy the Co-FM phase can achieve positive magnetization, and there is the third compensation temperature at $T_3 \simeq 78$ K. Finally, there are the transitions of the Co^{2+}-AFM and Co^{2+}/Co^{3+}-FM phases to the paramagnetic state.

This behavior is closely related to the dynamics of the spin clusters, which are strongly dependent on H_{dc} and measurement time. For different times of measurement, the compensation temperatures can vary. For a larger H_{dc}, the system achieves positive magnetization values already at low T, and there is no magnetic reversal, as can be observed on Fig. 2(b) for the curve measured under $H_{dc} = 1000$ Oe. On the other hand, for small H_{dc} the SG peak is not large enough to achieve the positive magnetization and the system undergoes only to one compensation temperature, T_3. For $H_{dc} = 200$ Oe, one have $T_3 = 92$ K, as shown in Fig. 2(b). Another important result obtained from Fig. 2(b) is that the low T peak maxima shifts to lower-T as H_{dc} increases. For $H_{dc} = 200, 500$, and 1000 Oe the peak maxima are located at 27.8, 25.4, and 23.9 K, respectively. This is an expected feature of a SG-like material, as will be discussed next.

The ac magnetic susceptibility (χ_{ac}) was measured as a function of T for seven frequencies in the range $10 - 10^4$ Hz. Figure 3(a) shows the real (χ'_{ac}) and imaginary (χ''_{ac}) parts of susceptibility for some selected frequencies. For χ'_{ac}, it was observed for the low-T peak (T_f) a systematic shift of T_f to higher-T with the increase of driving frequency, where T_f shift from 27 K at 10 Hz to 27.84 K at 10^4 Hz. It was also observed a decrease of the peak amplitude with increasing frequency. Both results are characteristic of SG-like materials. On the other hand, for the $T \simeq 90$ K only a small amplitude decrease was observed at higher frequencies, but no measurable shift, which characterizes ordinary magnetic transitions.

The frequency-dependent data turn out to be well described by the conventional critical slowing down model of the dynamic scaling theory [3,46,47], which predicts a power law

$$\frac{\tau}{\tau_0} = \left[\frac{(T_f - T_{sg})}{T_{sg}} \right]^{-z\nu}, \quad (4)$$

where τ is the relaxation time corresponding to the measured frequency, τ_0 is the characteristic relaxation time of spin flip, T_{sg} is the SG transition temperature (as frequency tends to zero), z is the dynamical critical exponent and ν is the critical exponent of the correlation length. The solid line in the inset of Fig. 3(a) represents the best fit to the power law divergence, that yields $T_{sg} = 26.6$ K, $\tau_0 = 1.5 \times 10^{-13}$ s, and $z\nu = 6.5$. These results are in the realm of conventional SG phases.

A criterion that is often used to compare the frequency dependence of T_f in different SG systems is to compare the
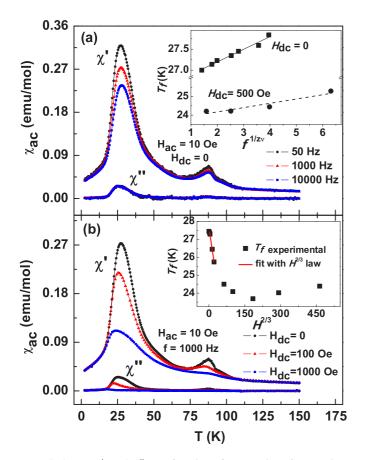
FIG. 3. (a) χ'_{ac} and χ''_{ac} as a function of T at various frequencies. The inset shows T_f as a function of frequency for $H_{dc} = 0$ and 500 Oe, obtained from χ'_{ac}. The lines are best fits to the power law $T_f = T_{sg}[1 + (\tau_0 f)^{1/z\nu}]$. (b) χ'_{ac} and χ''_{ac} vs T at $f = 1000$ Hz for various H_{dc}. Inset shows T_f for different applied H_{dc}.

relative shift in T_f per decade of frequency

$$\delta T_f = \frac{\triangle T_f}{T_f \, \triangle (\ln f)}. \tag{5}$$

For La$_{1.5}$Ca$_{0.5}$CoIrO$_6$, we found $\delta T_f \simeq 0.008$, which is within the range usually found for conventional SG ($\delta T_f \lesssim 0.01$). For superparamagnets, the usual value is $\delta T_f \gtrsim 0.1$, while for cluster glasses (CG), it has intermediate values between canonical SG and superparamagnets [3,45,46,48].

The SG cusps on Fig. 3(a) are broader than usually observed for canonical SG. Since La$_{1.5}$Ca$_{0.5}$CoIrO$_6$ is a RSG material, this may be due to the internal molecular field resulting from Co moments. In order to verify the field effect on the magnetization, it was measured χ_{ac} with $H_{dc} = 500$ Oe. The inset of Fig. 3(a) shows that, for this H_{dc}, T_f also shifts to higher-T with increasing frequency. The dashed line is the fit to the power law, yielding $T_{sg}^{500\,Oe} = 23.7$ K, $z\nu = 5$, $f_0 = 10^{10}$ Hz. With $H_{dc} = 500$ Oe, the relative shift in T_f [Eq. (5)] increases to $\delta T_f \simeq 0.01$. All these results are compatible to those usually reported for CG materials. Hence H_{dc} induces the increase of the correlation length of the spin clusters, i.e., there is a transition from SG to CG in the system.

Figure 3(b) shows χ'_{ac} and χ''_{ac} measurements for fixed $f = 1000$ Hz and $H_{ac} = 10$ Oe, but different H_{dc}. As expected,
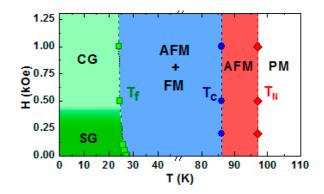

FIG. 4. Temperature-field phase diagram showing the Néel (T_N), critical (T_C), and freezing (T_f) temperatures of La$_{1.5}$Ca$_{0.5}$CoIrO$_6$. The lines are guides for the eye.

the SG peak is smeared out and shifts to lower-T with increasing H_{dc} [3]. The inset shows that $T_f(H)$ reasonably follows the $H^{2/3}$ Almeida-Thouless relation [49] for $H_{dc} \lesssim 100$ Oe, and the curve's slope changes for higher fields. Since La$_{1.5}$Ca$_{0.5}$CoIrO$_6$ is a RSG compound, H_{dc} have its effect on the underlying Co ions, inducing the transition from conventional SG to CG. This result may bring important insights about the effect of strong H_{dc} on the frozen spins and also on the limit of validity of the $H^{2/3}$ relation for a RSG. H_{dc} seems to remove the criticality of the transition, yet it does not fully prevent the formation of the frozen state [3].

In contrast to χ'_{ac}, for χ''_{ac}, there was a small nonmonotonic variation of the peak position and amplitude. This is an unconventional behavior for a SG-like material, and it was not found a reasonable simple explanation for it. It was already reported for the ternary intermetallic CeRhSn$_3$ a shift toward lower-T with increasing frequency [45,50]. But differently than for La$_{1.5}$Ca$_{0.5}$CoIrO$_6$, the shift was on χ', while χ'' goes to higher-T with increasing frequency. Here is important to stress that, despite the fact our measurements were carefully taken, the overall smaller and more noisy χ''_{ac} makes it more difficult to precisely determine the T_f position, specially for lower frequencies.

The complex magnetic behavior of La$_{1.5}$Ca$_{0.5}$CoIrO$_6$ can be summarized in a rich phase diagram, showing its conventional and SG-like states. Figure 4 displays the field-temperature phase diagram for the compound, where can be observed its Néel temperature (T_N) at $T_N \simeq 97$ K, its critical temperature (T_C) at $T_C \simeq 86$ K, and its freezing temperature (T_f) at $T_f \simeq 26.6$ K. An important result observed is that, depending on H_{dc}, at low-T the material can behave as a conventional spin glass or as a cluster glass.

C. Exchange bias

$M(H)$ curves for ordinary FM and FIM materials usually exhibit hysteretic behavior with coercive field due to the blocking of the domain wall motion. In SG-like materials, irreversibility can also be observed arising out of anisotropy [3,51,52]. Hence, in a RSG system a large anisotropic coercivity can be expected due to the combined action of FM, AFM and SG phases. The ZFC $M(H)$ measurements were performed for several T using a systematic protocol detailed

in Ref. [30], and two representative curves are displayed in Fig. 5(a), where one can see a small increase in the magnetization from 5 to 15 K. The increase of thermal energy results in an enhancement of the SG alignment to the field direction, yielding in a larger magnetization. However, due to thermal energy, these spins can flip to the field direction, leading to the observed decrease of coercivity. It is also important to note that the system exhibit a non-negligible M_{sp} at zero field [inset of Fig. 5(a)]. This M_{sp} shows a systematic evolution with T, and plays an important role on the process of pinning the spins, as it will be discussed next.

Here we define the EB field as $H_{EB} = |H_+ + H_-|/2$, where H_+ and H_- represent the right and left field values of the $M(H)$ loop at the $M = 0$ axis, respectively. The effective coercive field is $H_C = |H_+ - H_-|/2$. Usually, the EB effect is achieved when the system is cooled in the presence of nonzero H_{dc}. Interestingly, for $La_{1.5}Ca_{0.5}CoIrO_6$ a non-negligible shift of the hysteresis loop is observed even when the system is cooled in zero field. This spontaneous EB effect, also called zero field cooled EB (ZEB), was recently reported for distinct systems such as Mn_2PtGa [53] and Ni-Mn-In [54] alloys, and the nanocomposite $BiFeO_3$-$Bi_2Fe_4O_9$ [55]. Therefore, here we have found, to the best of our knowledge, the first example of a material to have this phenomenon clearly related to three distinct magnetic phases, namely FM, AFM, and SG. At 2 K, $La_{1.5}Ca_{0.5}CoIrO_6$ exhibit a negative shift $H_{ZEB} \simeq 290$ Oe. In order to verify this effect we have measured $M(H)$ with the initial H_{dc} in the opposite direction. As can be observed on Fig. 5(b), the curve exhibits a positive shift $H_{ZEB} \simeq 135$ Oe. The shift in the opposite direction is an expected behavior of a EB system, hence a clear evidence that this result is intrinsic of the material. The fact that H_{ZEB} is different depending on the direction of the initial magnetization process is an indicative that the internal M_{sp} plays an important role in the pinning of the spins.

$La_{1.5}Ca_{0.5}CoIrO_6$ presents FM and SG phases incorporated to an AFM matrix. Due to its predominant AFM phase, it does not saturate even at a large field of 9 T. As will be discussed next, the ZEB effect here observed results from the a delicate exchange interaction on the interfaces of the AFM/SG phases to the minor FM phase. Hence, for large enough applied fields, the pinned spins at the interface may flip to the field direction, reducing the effect. This is actually what is observed for fields larger than 4 T. For instance, for a maximum applied field (H_m) of 9 T, the EB effect is reduced to $H_{ZEB} = 40$ Oe. In order to evidence the FM contribution to the $M(H)$ curves, the AFM contribution was subtracted from the loops. The linear curve representing the AFM phase was obtained from the fit of the loops at high fields, which was extrapolated to the whole field range and then subtracted from the loop. The resulting curve obtained for $T = 5$ K is displayed in Fig. 5(c). It is almost symmetric in respect to the M axis and displays the same H_{ZEB} as that obtained from the original curve. It must be mentioned that the resulting curves contemplate both the contributions of the FM and SG phases, i.e., it is not possible to separate these phases on the curves.

Despite the ZEB being an effect only recently reported, the conventional exchange-bias (CEB) is a well known phenomenon encountered in systems containing interfaces between distinct magnetic phases, being most likely found in
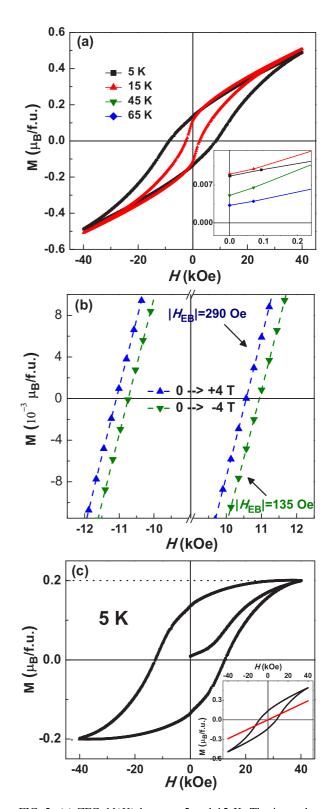

FIG. 5. (a) ZFC $M(H)$ loops at 5 and 15 K. The inset shows a magnified view of the initial magnetization values at zero field. (b) ZFC $M(H)$ loops at 2 K performed as $0 \rightarrow 4\,T \rightarrow -4\,T \rightarrow 4\,T$ and $0 \rightarrow -4\,T \rightarrow 4\,T \rightarrow -4\,T$. (c) FM + SG contributions to the $M(H)$ loop at $T = 5$ K. The doted lines are guides for the eye. The inset shows the original curve and the linear AFM contribution (see text).
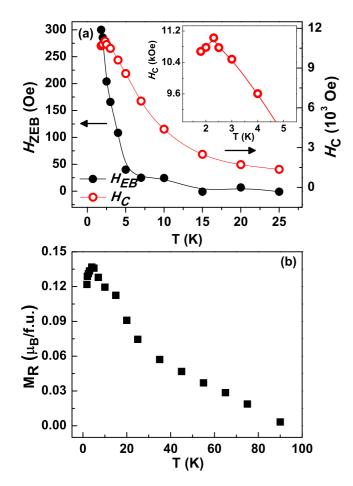
FIG. 6. (a) H_{ZEB} and H_C evolution with T. The inset shows a magnified view of the low-T anomaly on H_C. The lines are guides for the eye. (b) M_R dependency with T.

FM-AFM systems. But a shift of the magnetization hysteresis loops along the field axis can be also observed in situations not related to EB effect. In a conventional FM material, if a minor $M(H)$ loop is measured, i.e., an $M(H)$ with the maximum applied field not large enough to the system achieve the magnetic saturation, it can exhibit a shift along the field axis similar to that observed in EB systems. This is in general related to the incomplete magnetic reversal of the system [56,57]. However, differently than observed in EB materials, these minor loops also exhibit a large shift along the magnetization axis, and in general the loops are not closed at large fields [58,59]. As Fig. 5 shows, $M(H)$ of La$_{1.5}$Ca$_{0.5}$CoIrO$_6$ is a closed loop with a very small shift along the vertical axis due to the pinned spins, as expected. It is a indicative that ZEB reported here is not due to a minor loop hysteresis. In order to reinforce the difference between the curves here observed from those obtained from minor loops, we compare in Ref. [30] the results here described with that obtained from true minor loops.

The evolution of H_{ZEB} and H_C with T are displayed on Fig. 6(a). One can observe that the ZEB effect can only be achieved below T_f. Moreover, it rapidly decreases with the enhancement of the thermal energy. Usually, a decrease in the magnetic unidirectional anisotropy (UA) is associated with an increase of the coercivity [10]. Hence, the low-T anomaly

observed for H_C on inset of Fig. 6(a) is another expected feature of EB systems.

Different mechanisms are invoked to explain the ZEB for distinct materials. For instance, for Ni-Mn-In it is proposed that the UA is formed at the interface between different magnetic phases during the initial magnetization process of $M(H)$ curves [54]. On the other hand, for BiFeO$_3$-Bi$_2$Fe$_4$O$_4$ it is proposed that glassy moment at the interface between FM-AFM phases causes the EB effect [55]. Despite the distinct mechanisms claimed to be the responsible for the ZEB effect on each compound, they all have in common the RSG behavior. Here we conjecture that the internal molecular field plays an important role on the ZEB effect. We propose the following mechanism to explain the ZEB effect on La$_{1.5}$Ca$_{0.5}$CoIrO$_6$. The internal field due to the FM phase have its impact on AFM and SG phases. It affects the correlation length of the SG clusters, favoring the freezing of the glassy spins in the same direction, resulting in a spontaneous UA. The ZEB is enhanced by H_{dc} during the initial magnetization process of the $M(H)$ loop. The field induces the increase of the internal interaction of FM domains, leading to the growth of the spin clusters. After the removal of H_{dc}, the spins at the grain interfaces are pinned, resulting in a stable magnetic phase with UA at low T. As T increases the pinned spins can easier flip to the field direction due to the enhanced thermal energy. This leads to the reduction of H_{ZEB} and the correlated increase of H_C observed on Fig. 6(a).

The same scenario can explain the system's remanent magnetization, $M_R = |M_R^+ - M_R^-|/2$, where M_R^+ and M_R^- are the positive and negative values of the magnetization at zero field. Figure 6(b) displays the M_R evolution with T. On going from low to high T, first there is an increase of M_R due to the thermally activated movement of the spins to the field direction. Then going to higher T there is the continuous decrease of M_R until it vanishes at the paramagnetic sate. It is important to observe that despite the fact the FM phase orders at ~90 K, the ZEB effect only occurs below T_f. This, together with the fact that at low-T M_R and H_C initially increase while H_{EB} decreases on increasing T, are other evidences that the ZEB observed is strongly related to the RSG state and is not due to some minor hysteresis loop of the FM phase.

As addressed above, a significant evidence that the observed ZEB effect on La$_{1.5}$Ca$_{0.5}$CoIrO$_6$ is not due to some experimental artifact is the fact that the $M(H)$ loops shift to opposite directions depending on the initial applied field be positive or negative. If there were remanent current on the magnet due to an trapped flux or any other reason, both shifts should be expected to be in the same direction. This inversion of H_{EB} depending on the initial field value is also observed when the CEB effect is measured, i.e., when the isothermal $M(H)$ curve is measured after the system being field cooled. Figure 7(a) displays the $M(H)$ loop with $H_m = 7$ T, after the sample being cooled in the presence of $H_{FC} = 3$ T. The AFM contribution is also displayed, and the inset shows the deconvoluted curve, i.e., the resulting curve when the AFM one is subtracted. In Fig. 7(b), is shown a magnified view of the 2-K loops after the sample being cooled with $H_{FC} = \pm 3$ T. Differently than for the ZEB curves, for CEB the two curves are nearly symmetrically displaced with respect to the magnetization axis. Here the ± 3-T cooling field is strong enough to flip the spontaneous
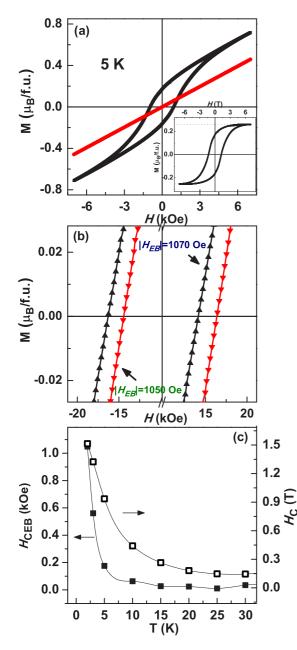
FIG. 7. (a) $M(H)$ loop at 5 K after cooling the system with $H_{FC} =$ 3 T. The inset shows the deconvolute curve (see text). (b) Magnified view of the curves measured at 2 K after the sample being field cooled with $H_{FC} \pm 3$ T. (c) H_{CEB} and H_C evolution with T.

magnetization, and the effect of the internal field becomes negligible.

Figure 7(c) shows the temperature dependence of H_{CEB} and H_C. The CEB evolution is similar to ZEB. Above T_f the H_{CEB} becomes negligible. It shows the importance of the SG phase to the EB observed on La$_{1.5}$Ca$_{0.5}$CoIrO$_6$. It can be also observed that the EB effect is greatly enhanced when the system is field cooled. At 2 K, one have $H_{CEB} \simeq 1070$ Oe. On the FC procedure, the pinning of the SG spins is favored already from above T_f down to low T, and these spins get frozen on the field direction.
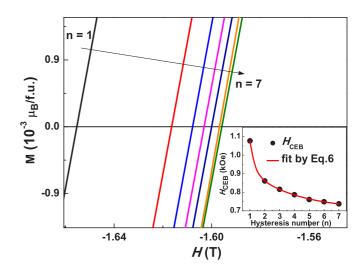

FIG. 8. Training effect of CEB at 2 K. The inset shows H_{CEB} as a function of the hysteresis number (n). The solid line represents the fitting of the experimental data to Eq. (6).

In EB systems, repeating the $M(H)$ loop may lead to relaxation of uncompensated spin configuration at the interface. Consequently, H_{EB} depends on the number of consecutive hysteresis loops measured. This property is called training effect. For La$_{1.5}$Ca$_{0.5}$CoIrO$_6$, this behavior was investigated in both ZEB and CEB cases. For CEB, seven consecutive loops were measured at 2 K, after cooling the sample in the presence of $H_{FC} = 3$ T. Figure 8 shows a detailed view of the seven loops close to the $M = 0$ axis. The arrow indicates a systematic evolution of the curves. The dependence of H_{CEB} on the number of repeating cycles (n) is shown on inset. As can be observed, H_{CEB} decreases monotonically with the increase in n, indicating spin rearrangement at the interface. The n dependence of H_{CEB} can be fit to a model considering the contribution of both the frozen spins and the uncompensated rotatable spins at the interface [55,60]

$$H_{CEB}^n = H_{CEB}^{\infty} + A_f e^{(-n/P_f)} + A_r e^{(-n/P_r)}, \quad (6)$$

where f and r denote the frozen and rotatable spin components, respectively. Equation (6) fits the data very well, for $H_{CEB}^{\infty} = 708$ Oe, $A_f = 4627$ Oe, $P_f = 0.3$, $A_r = 282$ Oe, and $P_3 = 3.1$. The fact $A_f > A_r$ indicates the importance of the SG phase to the EB effect, and $P_r > P_f$ suggests that the rotatable spins rearrange faster than the frozen ones. For the ZEB mode, it was observed only a very small decrease of H_{ZEB} from first to second loop, thereafter the system exhibits only negligible variation. This indicates that after the first cycle, the frozen and uncompensated spins became quite stable at the interfaces.

IV. CONCLUSIONS AND OUTLOOK

In conclusion, we have shown that La$_{1.5}$Ca$_{0.5}$CoIrO$_6$ is an RSG-like material, in which there are two magnetic orderings of the AFM and FM phases of Co ions at $T_N = 97$ K and $T_C = 86$ K, respectively, and an SG-like transition at $T_{sg} = 26.6$ K. The frequency dependence of T_f obtained from χ_{ac}' follows the power law of the dynamical scaling theory.

Regarding the χ_{ac} measurements with applied H_{dc} fields, the system transits from conventional spin glass to cluster glass with increasing H_{dc}. The coexistence of conventional and glassy magnetic states leads to an exotic magnetic behavior in the ZFC T-dependence of magnetization curve, in which the system can undergo three magnetic reversals. Magnetization as a function of H_{dc} suggests an ZEB effect at low T, related to the FM-AFM-SG interfaces. When the sample is cooled in the presence of an applied magnetic field, the EB effect is enhanced. XPS, XANES, XMCD, and electronic structure calculations results corroborate our argument that the magnetization reversals and the EB effect can be both understood in terms of the same underlying mechanism, i.e., are consequences of the Ir magnetic frustration caused by the competing interactions with its neighboring Co ions. To verify these and other conjectures discussed in the text, other techniques such as neutron scattering, torque magnetometry and electronic spin resonance are necessary.

[1] J. Knolle, G.-W. Chern, D. L. Kovrizhin, R. Moessner, and N. B. Perkins, Phys. Rev. Lett. **113**, 187201 (2014).

[2] K. Binder and A. P. Young, Rev. Mod. Phys. **58**, 801 (1986).

[3] J. A. Mydosh, *Spin Glasses: An Experimental Introduction* (Taylor & Francis, London, 1993).

[4] D. K. Singh and Y. S. Lee, Phys. Rev. Lett. **109**, 247201 (2012).

[5] J. E. Greedan, J. Mater. Chem. **11**, 37 (2001).

[6] J. M. De Teresa, M. R. Ibarra, J. García, J. Blasco, C. Ritter, P. A. Algarabel, C. Marquina, and A. del Moral, Phys. Rev. Lett. **76**, 3392 (1996).

[7] A. K. Kundu, P. Nordblad, and C. N. R. Rao, Phys. Rev. B **72**, 144423 (2005).

[8] Q. Xu, Y. Sheng, M. Khalid, Y. Cao, Y. Wang, X. Qiu, W. Zhang, M. He, S. Wang, S. Zhou, Q. Li, D. Wu, Y. Zhai, W. Liu, P. Wang, Y. B. Xu, and J. Du, Sci. Rep. **5**, 9093 (2015).

[9] D. Niebieskikwiat and M. B. Salamon, Phys. Rev. B **72**, 174422 (2005).

[10] J. Nogués and I. K. Schuller, J. Magn. Magn. Mater. **192**, 203 (1999).

[11] M. Ali, P. Adie, C. H. Marrows, D. Greig, B. Hickey, and R. L. Stamps, Nat. Mater. **6**, 70 (2007).

[12] M. Gruyters, Phys. Rev. Lett. **95**, 077204 (2005).

[13] L. T. Coutrim, D. C. Freitas, M. B. Fontes, E. Baggio-Saitovitch, E. M. Bittar, E. Granado, P. G. Pagliuso, and L. Bufaiçal, J. Solid State Chem. **221**, 373 (2015).

[14] A. Kolchinskaya, P. Komissinskiy, M. Baghaie Yazdi, M. Vafaee, D. Mikhailova, N. Narayanan, H. Ehrenberg, F. Wilhelm, A. Rogalev, and L. Alff, Phys. Rev. B **85**, 224422 (2012).

[15] J. C. Cezar, N. M. Souza-Neto, C. Piamonteze, E. Tamura, F. Garcia, E. J. Carvalho, R. T. Neueschwander, A. Y. Ramos, H. C. N. Tolentino, A. Caneiro, N. E. Massa, M. J. Martinez-Lope, J. A. Alonso, and J. Itie, J. Synchrotron Radiat. **17**, 93 (2010).

[16] B. Ravel and M. Newville, J. Synchrotron Radiat. **12**, 537 (2005).

[17] P. Blaha, K. Schwarz, G. K. H. Madsen, D. Kvasnicka, and J. Luitz, WIEN2K, *An Augmented Plane Wave + Local Orbitals Program for Calculating Crystal Properties* (Karlheinz Schwarz, Techn. Universitat Wien, Austria, 2001).

[18] S. C. Petitto, E. M. Marsh, G. A. Carson, and M. A. Langell, J. Mol. Catal. A: Chem. **281**, 49 (2008).

[19] J. van Elp, J. L. Wieland, H. Eskes, P. Kuiper, G. A. Sawatzky, F. M. F. de Groot, and T. S. Turner, Phys. Rev. B **44**, 6090 (1991).

[20] V. M. Jimenez, A. Fernandez, J. P. Espinos, and A. R. Gonzalez-Elipe, J. Electron. Spectrosc. Relat. Phenom. **71**, 61 (1995).

[21] M. Hassel and H.-J. Freund, Surf. Sci. Spectra **4**, 273 (1996).

[22] C. A. F. Vaz, D. Prabhakaran, E. I. Altman, and V. E. Henrich, Phys. Rev. B **80**, 155457 (2009).

[23] C. R. Brundle, T. J. Chuang, and D. W. Rice, Surf. Sci. **60**, 286 (1976).

[24] R. P. Gupta and S. K. Sen, Phys. Rev. B **12**, 15 (1975).

[25] T. Ivanova, A. Naumkin, A. Sidorov, I. Eremenko, and M. Kiskin, J. Electron. Spectrosc. Relat. Phenom. **156-158**, 200 (2007).

[26] M. C. Biesinger, B. P. Payne, A. P. Grosvenor, L. W. M. Lau, A. R. Gerson, and R. St. C. Smart, Appl. Surf. Sci. **257**, 2717 (2011).

[27] B. Raveau and Md. Motin Seikh, *Cobalt Oxides: From Crystal Chemistry to Physics* (Wiley-VCH, Weinheim, 2012).

[28] T. C. Koethe, Ph.D. thesis, Universität zu Köln, 2007.

[29] D. Niebieskikwiat, R. D. Sánchez, A. Caneiro, L. Morales, M. Vásquez-Mansilla, F. Rivadulla, and L. E. Hueso, Phys. Rev. B **62**, 3340 (2000).

[30] See Supplemental Material at http://link.aps.org/supplemental/10.1103/PhysRevB.93.174406 for details of the magnetometry results, x-ray near edge structure (XANES), x-ray magnetic circular dichroism (XMCD), and electronic structure calculations, which includes Refs. [31–37].

[31] T. Dey, A. Maljuk, D. V. Efremov, O. Kataeva, S. Gass, C. G. F. Blum, F. Steckel, D. Gruner, T. Ritschel, A. U. B. Wolter, J. Geck, C. Hess, K. Koepernik, J. van den Brink, S. Wurmehl, and B. Büchner, Phys. Rev. B **93**, 014434 (2016).

[32] J. Stöhr and H. König, Phys. Rev. Lett. **75**, 3748 (1995).

[33] B. T. Thole, P. Carra, F. Sette, and G. van der Laan, Phys. Rev. Lett. **68**, 1943 (1992).

[34] P. Carra, B. T. Thole, M. Altarelli, and X. Wang, Phys. Rev. Lett. **70**, 694 (1993).

[35] C. T. Chen, Y. U. Idzerda, H.-J. Lin, N. V. Smith, G. Meigs, E. Chaban, G. H. Ho, E. Pellegrin, and F. Sette, Phys. Rev. Lett. **75**, 152 (1995).

[36] J. P. Perdew, A. Ruzsinszky, G. I. Csonka, O. A. Vydrov, G. E. Scuseria, L. A. Constantin, X. Zhou, and K. Burke, Phys. Rev. Lett. **100**, 136406 (2008).

[37] I. D. Seymour, A. Chroneos, J. A. Kilner, and R. W. Grimes, Phys. Chem. Chem. Phys. **13**, 15305 (2011).

[38] M. Dlouhá, J. Hejtmánek, Z. Jirák, K. Knízek, P. Tomes, and S. Vratislav, J. Magn. Magn. Mater. **322**, 1189 (2010).

[39] P. D. Battle, J. G. Gore, R. C. Hollyman, and A. V. Powell, J. Alloys Compd. **218**, 110 (1995).

[40] J. B. Goodenough, *Magnetism and Chemical Bond* (Interscience, New York, 1963).

[41] Housung Seo, Agham Posadas, and Alexander A. Demkov, Phys. Rev. B **86**, 014430 (2012).

[42] S.-W. Kim, C. Liu, H.-J. Kim, J.-H. Lee, Y. Yao, K.-M. Ho, and J.-H. Cho, Phys. Rev. Lett. **115**, 096401 (2015).

[43] Md. Motin Seikh, Ch. Simon, V. Caignaert, V. Pralong, M. B. Lepetit, S. Boudin, and B. Raveau, Chem. Mater. **20**, 231 (2008).

[44] H. Singh, H. Ghosh, T. V. Chandrasekhar Rao, A. K. Sinha, and P. Rajput, J. Appl. Phys. **116**, 214106 (2014).

[45] V. K. Anand, D. T. Adroja, and A. D. Hillier, Phys. Rev. B **85**, 014418 (2012).

[46] J. Souletie and J. L. Tholence, Phys. Rev. B **32**, 516(R) (1985).

[47] P. C. Hohenberg and B. I. Halperin, Rev. Mod. Phys. **49**, 435 (1977).

[48] A. Malinowski, V. L. Bezusyy, R. Minikayev, P. Dziawa, Y. Syryanyy, and M. Sawicki, Phys. Rev. B **84**, 024409 (2011).

[49] J. R. L. Almeida and D. J. Thouless, J. Phys. A **11**, 983 (1978).

[50] V. K. Anand, D. T. Adroja, A. D. Hillier, W. Kockelmann, A. Fraile, and A. M. Strydom, J. Phys. Condens. Matter **23**, 276001 (2011).

[51] S. Mukherjee, R. Ranganathan, P. S. Anilkumar, and P. A. Joy, Phys. Rev. B **54**, 9267 (1996).

[52] K. De, M. Patra, S. Majumdar, and S. Giri, J. Phys. D: Appl. Phys. **40**, 7614 (2007).

[53] A. K. Nayak, M. Nicklas, S. Chadov, C. Shekhar, Y. Skourski, J. Winterlik, and C. Felser, Phys. Rev. Lett. **110**, 127204 (2013).

[54] B. M. Wang, Y. Liu, P. Ren, B. Xia, K. B. Ruan, J. B. Yi, J. Ding, X. G. Li, and L. Wang, Phys. Rev. Lett. **106**, 077203 (2011).

[55] T. Maity, S. Goswami, D. Bhattacharya, and S. Roy, Phys. Rev. Lett. **110**, 107201 (2013).

[56] J. J. Becker, IEEE Trans. Magn. **12**, 965 (1976).

[57] O. Benda, J. Bydzoviský, P. Krivosík, and E. Usák, J. Magn. Magn. Mater. **215**, 644 (2000).

[58] L. Pi, S. Zhang, S. Tan, and Y. Zhanga, Appl. Phys. Lett. **88**, 102502 (2006).

[59] L. Klein, Appl. Phys. Lett. **89**, 036101 (2006).

[60] S. K. Mishra, F. Radu, H. A. Durr, and W. Eberhardt, Phys. Rev. Lett. **102**, 177208 (2009).